

Challenging Problems on Ventilated Cavitation and Paths to Their Computational Solutions

E. L. Amromin¹

Received: 3 October 2018 / Accepted: 29 November 2018 / Published online: 22 July 2019
© Harbin Engineering University and Springer-Verlag GmbH Germany, part of Springer Nature 2019

Abstract

Ventilated cavitation has been successfully employed as ship drag reduction technology and potentially can mitigate flow-induced vibration. The obtained successes were based on solutions of design problems considered in the framework of ideal fluid theory with their following validation by towing tank tests. However, various aspects of the interaction of ventilated cavities with the viscous flows around the ship hulls remain unclear, whereas there is usually no possibility to simultaneously keep the full-scale Froude number and cavitation number in the test facilities. So, the further progress of the application of ventilated cavitation substantially depends on the ability of computational tools to predict this interaction. This paper briefly describes the state-of-the-art computation of ventilated cavitation and points out the most challenging unsolved problems that appeared in the model tests (prediction of air demand by cavities, ventilation effect on ship drag, on hydrofoil lift, and on the propagation of shock waves in cavities).

Keywords Ventilated cavitation · Computational fluid dynamics · Lift, drag, and air demand of cavitating bodies · Shock waves in cavities

1 Introduction

Ventilated cavitation has been initially employed as a substitute for natural cavitation in the low-velocity experimental facilities (after Reichardt 1945). During several following decades, ventilated cavitation has been used in the experiments with the simple shape bodies. In the same time, the single mathematical model employed for cavitating flows has been the theory of ideal fluid flows with free boundaries. The perfect description of this theory can be found in the book by Gurevich (1970). This theory did not separate ventilated cavitation from natural cavitation.

Later several types of ventilated flows have been successfully employed for improvement of ships, underwater

vehicles, or their tested models. The successful application of ventilated cavitation to drag reduction of a river ship was first noted by Basin et al. (1969). Butuzov et al. (1990), Latorre (1997), Foeth (2008), Thill (2010), and Sverchkov (2010) described its application to other ships.

Ship drag reduction by bottom-ventilated cavitation became possible due to the contribution of two scientists. The first of them was Alexander Ivanov, who pointed out that such drag reduction can be possible only with the elimination of the drag penalty caused by oscillation of the cavity tail; so, the ship hulls must have some cavity lockers that can suppress these oscillations. The second was Anatoly Butuzov. The dependency of maximum cavity length on the Froude number was found by Butuzov (1966). As illustrated in Fig. 1, two kinds of bottom cavities for two kinds of the ship were invented. The “smooth” cavity could exist at any Froude number Fr , but its length is always smaller than the half wavelength $\Lambda/2 = \pi V^2/g$, where V is the ship speed. The broadest practical application of this kind of ventilated cavitation has been obtained in planning boats.

On the other hand, as explained and illustrated by Gorbachev and Amromin (2012), the “wavy” cavities can exist only at small Froude numbers. For both kinds of cavities, as shown in Fig. 2 with the images from Amromin et al.

Article Highlights

- This paper briefly describes the state-of-the-art computation of ventilated cavitation.
- It points out the most challenging unsolved problems that appeared in the model tests.

✉ E. L. Amromin
amromin@aol.com

¹ Mechmath LLC, Federal Way, WA 98003, USA

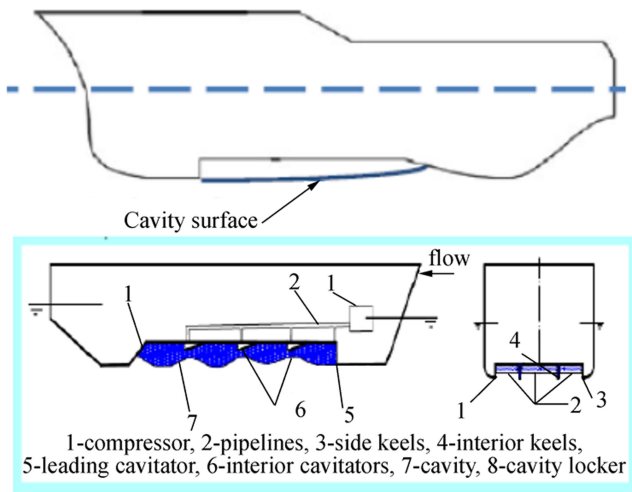


Fig. 1 Sketches of ship buttocks with “smooth” ventilated cavity (top) and “wavy” ventilated cavity

(2011) in its upper part and from Gorbachev et al. (2015) in its lower part, the very important design aspect is the design of the cavity locker. As one can see in the experimental data of Courouble (1971), the air demand by the bottom cavities without lockers is too high and requires unacceptable energy consumption.

However, the most sounding concept associated with drag reduction by ventilated cavitation is supercavitation over underwater missiles. Information on ventilation of underwater missiles exists at https://en.wikipedia.org/wiki/VA-111_Shkval. Here, this concept is clarified in Fig. 3. The cavity covers the major part of the body and eliminates the water friction on this part. Only two small areas at the body bow and its tail must be wetted to fix the cavity leading edge and to generate the vertical force compensating the body weight.

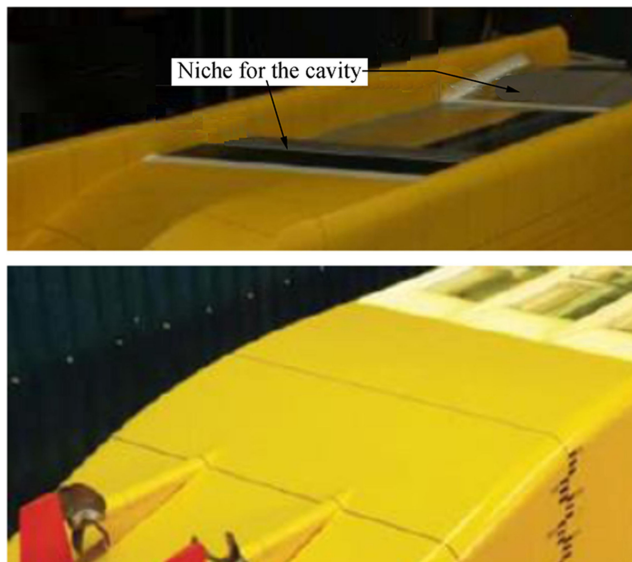


Fig. 2 Partial views of model bottoms with the cavity lockers; in the top—DTMB Model 5494 designed for $Fr = 0.5$; in the bottom—KSRC model designed for $Fr = 0.16$



Fig. 3 Sketch of a body surrounded by a ventilated cavity

The main challenge for this concept is the high drag penalty in supercavitating flows. It can be estimated using the dependency from Fig. 4 calculated with taking into account experimental data of Reichardt (1945). The drag penalty coefficient was normalized by the body surface there. This coefficient must visibly exceed the friction coefficient to make supercavitation useful. For natural cavitation, it would be possible at the speeds substantially exceeding 200 knots. Ventilation allows for drag reduction at the much smaller speeds, but the gas demand to maintain the cavity appears to be large, as was proven by Kuklinski et al. (2001), Kinzel et al. (2007), and others. As one can also find on the Internet, the gas supply issue was resolved for the SKVAL missile with the use of a special propulsor. However, the high pulsations of the supercavity tail result in the problems of motion control and high noise emission. It seems that these problems are unresolvable for supercavitating bodies.

Further, because of the buoyancy impact on cavity shapes at small and moderate values of Froude number, maintenance of ventilated cavities could be practical only under the bottoms of ships. However, Froude numbers related to wings of hydrofoil ships or to marine propeller blades can be big enough to neglect by this effect. On the other hand, the computational technique used for “smooth” cavities is applicable to problems on their drag reduction. The successful attempt of Amromin et al. (2006) to design a hydrofoil with drag reduction by partial cavitation is illustrated in Fig. 5. The designed hydrofoil OK2003 has the pressure side coinciding with the pressure side of the hydrofoil NACA0015, the concavity assigned for the cavity on the suction side, and the cavity locker downstream of this concavity. Such concavity is necessary because the cavity must be thick enough to withstand

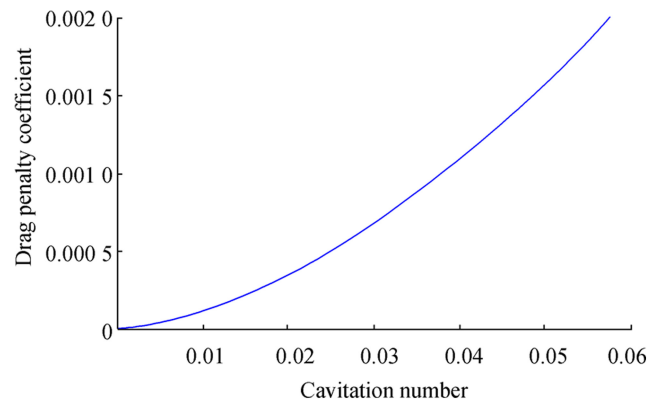
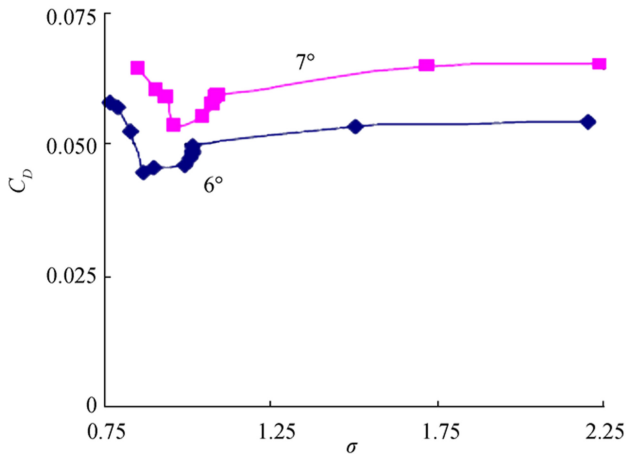


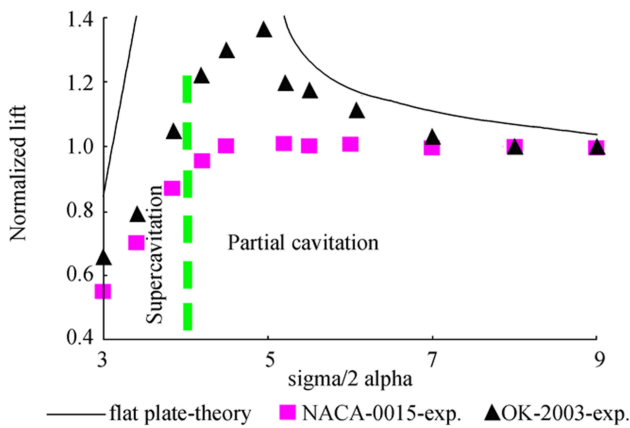
Fig. 4 Drag penalty coefficients for supercavitating bodies of revolution versus cavitation number



(a) View of the hydrofoil OK2003 in the water tunnel



(b) OK2003 drag coefficient versus cavitation number at two angles of attack α



(c) OK2003 its normalized lift in comparison with the lift of NACA 0015 and flat plate theory

Fig. 5 Features of hydrofoil OK2003. **a** View of the hydrofoil OK2003 in the water tunnel. **b** OK2003 drag coefficient versus cavitation number at two angles of attack α . **c** OK2003 its normalized lift in comparison with the lift of NACA 0015 and flat plate theory

moderate perturbations of the inflow. As seen in Fig. 5, this design gave a 20% to 25% drag reduction for both natural and ventilated cavitation with the very significant lift increase for natural cavitation at the design values of the angle of attack α and cavitation number σ .

Additionally, as shown in Fig. 6, this design leads to mitigation of the lift pulsations (and, correspondingly, of the flow-

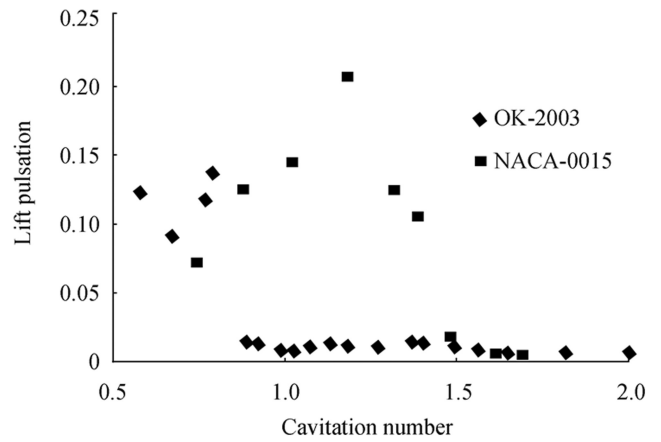


Fig. 6 Comparison of lift pulsation for hydrofoils OK2003 and NACA 0015

induced vibration) in the regime of partial cavitation. As shown in Fig. 7, this mitigation is more significant for ventilated cavitation. Alexander Ivanov suggested to employ ventilation for mitigation of the blade vibration in the 1980s, but the necessary blade design was not carried out then.

So, currently, ventilation is already used as the ship drag reduction technology. Prediction of the ship design result is based then on the towing tank tests. The similarity parameter in such tests is Froude number, whereas, for cavitating flows, the usual similarity parameter is cavitation number σ . Also, ventilated cavitation affects the boundary layers and therefore, the traditional extrapolations of viscous drag for cavitation-free hulls are not accurate enough here. Because of these circumstances, the extrapolation of the model test results to the full-scale conditions would be substantially improved by the computational analysis.

2 Computational Methods

Computational analysis in the framework of ideal incompressible fluid theory has played an important role in in the above-mentioned successes in applications of ventilated cavitation. However, the recent achievements of computational methods

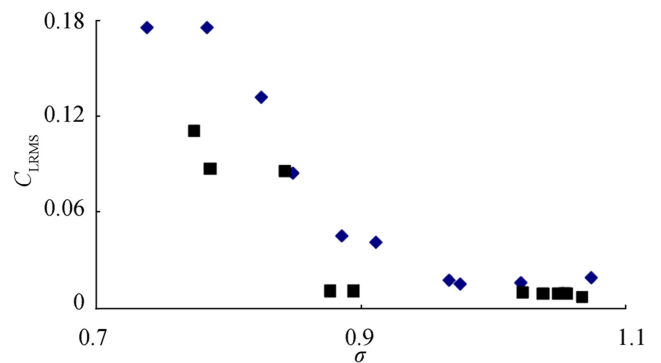


Fig. 7 Lift RMS for natural (rhombs) and ventilated (squares) cavitation of the hydrofoil OK2003 at $\alpha = 6^\circ$

for cavitating flows allow for their investigation in more detail. Indeed computational analysis of ventilated cavitation looks simpler than computational analysis of natural cavitation because lengths of ventilated cavities are comparable with the body lengths and are usually incomparably greater than the thickness of the body boundary layers. So, one zone solvers can be acceptable for the water flows around the ventilated cavities. As one can see in the recent review by Young et al. (2017), there are certain successes in studies of ventilated cavitation for hydrofoil and blades. Nevertheless, the challenges in computational analysis of ventilated cavitation remain and there are unsolved problems yet. These challenges and problems are the focus of this paper.

There are two groups of computational methods broadly employed in studies of ventilated cavitation. Only the very brief statements on their capabilities are provided here, but this is sufficient to understand the contemporary successes and challenges.

The first group of computational methods relates to the ideal fluid theory. The successful solution of the design problem can be delivered by ideal fluid theory. Indeed such a solution is a solution of the boundary-value problem for the velocity potential Φ :

$$\Delta\Phi = 0 \tag{1}$$

$$\partial\Phi/\partial N|_S = 0 \tag{2}$$

$$U^2 + 2P_c/\rho + 2g(z-z_\infty)|_{Sc} = U_\infty^2 + 2P_\infty/\rho \tag{3}$$

Here, $U = |\text{grad}(\Phi)|$; S in the combination of all boundaries of the flow; N is normal to S ; Sc is the cavity surface, P_∞ is the ambient pressure, and P_c is pressure in the cavity.

Problems (1)–(3) can be solved in the nonlinear approach, as by Amromin et al. (2006, 2011) or in the linear approach, as by Butuzov et al. (1990), Matveev (2007), Sverchkov (2010), and Gorbachev et al. (2015). These solutions allow for determination of the time-average cavity shapes. The average thickness of the cavity tail, drag penalty, and intensity of air escape are proportional to the computed cavity tail thickness (the examples are shown in Figs. 8 and 9). In particular, the minimal air demand to maintain cavity took place the model tests reported by Mäkiharju et al. (2010) for Position 1 at cavitation number $0.7 < \sigma < 0.72$. Our computational results in Figs. 8 and 9 are solutions of Eqs. (1)–(3) obtained in the nonlinear approach described in Amromin (2007), with illustrations of numerical verification of this approach.

As shown in Fig. 10, for smooth closure of the ventilated cavity (for a cavity without a drag penalty), the dependencies of pressure in the cavity on cavitation number must be kept, and this gives an implicit limitation on the air supply. As shown by Amromin and Arndt (2019), a combined analysis of incompressible ideal fluid flow out of the cavity and

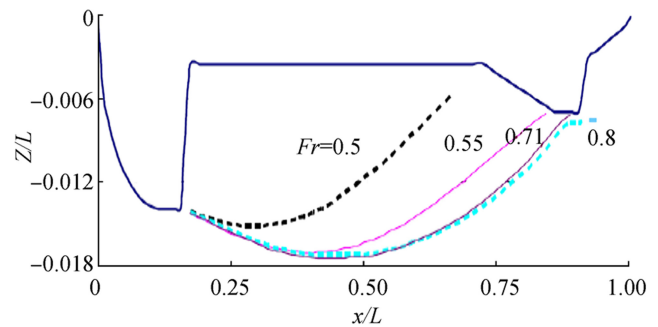


Fig. 8 Computed shapes of cavities maintained under the model tested by Mäkiharju et al. (2010). Solid thick line is its buttock corresponding to the beach Position 1. The cavity sections are plotted up to the time-average cavity tails

compressible ideal fluid flow inside the cavity allows for a quantitative prediction of forces on cavitating hydrofoils. However, there are also effects caused by the interaction of cavities with the surrounding viscous flow and these effects cannot be analyzed by ideal fluid theory.

The second group of computational methods relates to fully turbulent flows. For the majority of the employed designs, the viscous flow around and downstream of ventilated cavities is turbulent. The paper of Kinzel et al. (2007) gives a sufficient impression on the diversity of models of fully turbulent flows employed for computation of ventilated cavitation in the past. For natural cavitation, some of these models (like models used by Coutier-Delgosha et al. (2006), Kim (2015), and several others) manifested the satisfactory results.

No similar achievements were obtained for the ventilated cavities using the models of fully turbulent flows yet. For example, Ji et al. (2010), Wang et al. (2015), and Liu et al. (2018) show correlations of computed cavity regions with their snapshots for body cavitation for cavitating flows at very high Froude numbers. However, the comparisons of forces provide more certainty and are more important practically. Also, even similar results for much smaller Froude numbers (like provided by Abolfazl et al. (2012), f. e.) are uncommon. So, the ideal fluid theory methods (like used by Choi and Chahine (2010) or by Amromin (2018), f. e.) remain to be the most effective for ventilated cavitation yet.

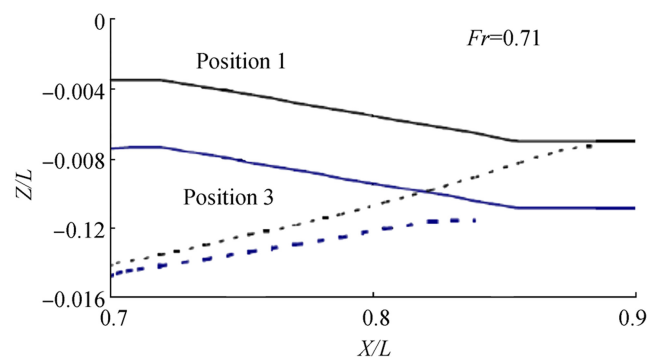


Fig. 9 Computed cavity tails (dashed curves) for two beach positions at the same Fr . The model buttocks—solid lines

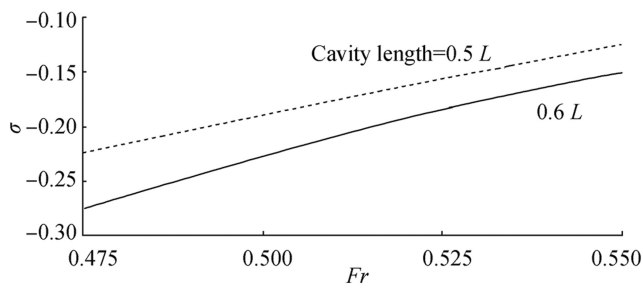


Fig. 10 Dependencies $Fr(\sigma)$ for cavities with smooth closure under Model 5494

This situation may be associated with the use of the flow model invented by Kubota et al. (1992) that substitutes any cavity by an ensemble of spherical bubbles. Meanwhile, as seen in Fig. 11 extracted from the paper of Wosnik et al. (2003), the main part of a ventilated cavity is not similar to an ensemble of bubbles. Also, the majority of solvers (like ANSYS employed by Long et al. (2017), f. e.) uses wall functions irrelevant to separated flows and are unable to reproduce velocity profiles across the cavities. This irrelevance must be fixed.

3 Unsolved Problems

Let us consider the most important problems associated with ventilated cavitation. This consideration is assisted by the presentation of unpublished experimental data and estimations.

3.1 Prediction of Air Demand

The energy spent to maintain the cavity must be substantially lower than the energy saved by ventilation. Its prediction is a challenge. There are numerous experimental studies of air demand for various models and ships, but the diversity of obtained experimental trends is disappointing.

As proven by observations of Arndt et al. (2009), for some designs, a ventilated cavity surrounded by laminar boundary layer can be maintained in a steady flow without any air supply. Thus, it looks that the turbulence impact on air entrainment from cavities is a very substantial effect. On the other hand, the increase of inflow speed in experiments was accompanied by the simultaneous increase Reynolds number Re and Fr . The air demand to maintain and create the cavity sharply increases at $Fr > 1$, but the cavity lockers for these experiments were designed for $Fr = 0.5$ and the cavity tail became thicker at $Fr > 1$. So, it is hard to identify the pure effects of



Fig. 11 Photo of a ventilated cavity

turbulence in these observations and measurements. Also, in the experiment with ventilated supercavities used by Kinzel et al. (2007), a sharp increase in air demand took place near the water tunnel blockage conditions. In the Epstein experiments noted by Kuklinski et al. (2001) the effect of Fr is coupled with the flow blockage effect. So, the substantial part of available experimental data relates to unpractical conditions. Nevertheless, air demand in some CFD studies is defined by approximation of suitable experimental data, as by Xiang et al. (2011).

The situation could be improved computationally, but though the attempt of Kinzel et al. (2007) to compute the air demand using various existing theories of turbulence was very informative, this attempt did not allow for determination of a single theory providing the trends similar to observed even in the mentioned experiments with a supercavitating body. The problem remains unsolved.

3.2 Prediction of Drag

As already noted in the Compendium (2015), the majority of drag reduction technologies reduces one drag component but increases another. Nevertheless, that note does not relate to drag reduction by ventilated cavitation.

As one can see in Fig. 12 with the experimental data of Amromin et al. (2011) for the Model 5494 shown in Fig. 2, the total drag reduction dR may exceed the friction eliminated by the cavity R_{friction} . In particular for the Model 5494, the physics behind of the high ratio dR/R_{friction} is the reduction of the hull side friction due to the significant heavy of the model hull in the ventilation regime. For the low-speed high-fullness model described by Gorbachev et al. (2015), this ratio was also bigger than 1.0 due to the reduction of the boundary layer thickness downstream of the cavity; this reduction results in a

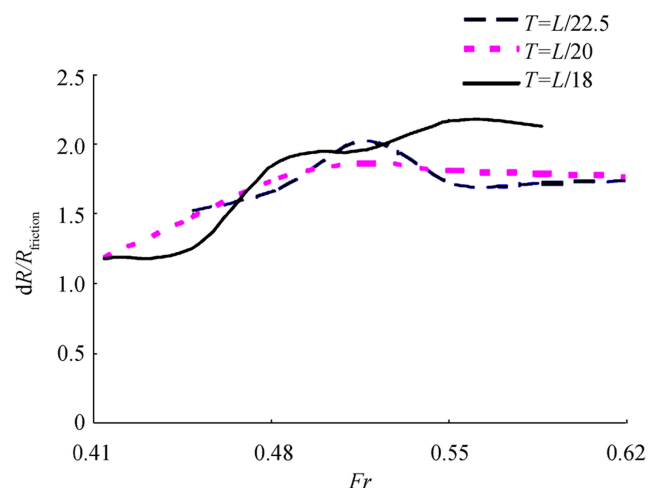


Fig. 12 Ratio of total drag reduction to friction eliminated by the cavity under Model 5494 at various ratios of its draft T to length L

decrease of the model form resistance. On the other hand, as reported by Zverkovski et al. (2014), this ratio may be below 1.0 for other hull designs.

However, currently, there is no computational tool capable to predict the drag for ships with ventilated bottom cavities. The situation with drag prediction is far from perfect for ventilated cavitating hydrofoils as well. In particular, there are no Reynolds-dependent numerical results for the hydrofoil OK2003 that has a quite high measured C_D at $Re = 8 \times 10^5$ (see Fig. 13). The shape of this hydrofoil is described in Tables 1 and 2.

By the way, because of the detailed experimental data for cavitating OK2003 presented in Figs. 5, 6, 13, and 14 and of other data published by Amromin et al. (2006) and Kopriva et al. (2007), this hydrofoil can be accepted as a benchmark for solvers developed for cavitating flows. The certain merit of such benchmark would be in the existence of experimental data for both natural and ventilated cavitation, as well as for the cavitation-free regime.

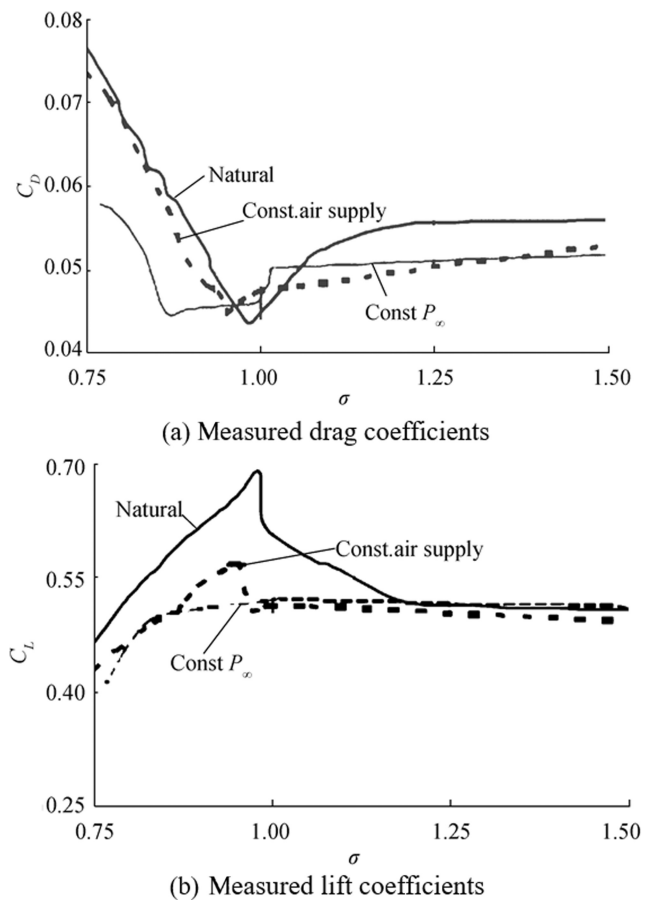


Fig. 13 Comparison of force coefficients for ventilated and naturally cavitating hydrofoil OK2003. **a** Measured drag coefficients. **b** Measured lift coefficients

Table 1 Upper side of hydrofoil OK2003

x/C	y/C	x/C	y/C
1	0	0.46158	0.079901
0.999605	9.88E-05	0.430062	0.06958
0.998901	0.000198	0.398556	0.058753
0.997901	0.000395	0.367037	0.047951
0.996395	0.000605	0.335519	0.037704
0.994099	0.001	0.304012	0.02858
0.990605	0.001605	0.272494	0.021099
0.985395	0.002605	0.240988	0.015802
0.977605	0.003901	0.209469	0.013247
0.965802	0.005901	0.177951	0.013099
0.934284	0.014235	0.146444	0.013099
0.902778	0.024383	0.114926	0.013099
0.871259	0.03516	0.08342	0.013099
0.839741	0.046111	0.051901	0.013099
0.808235	0.056877	0.034198	0.013099
0.776716	0.067173	0.022395	0.013099
0.745198	0.076753	0.014605	0.013099
0.713691	0.085432	0.009395	0.013099
0.682173	0.093062	0.005901	0.013099
0.650667	0.099457	0.003605	0.013099
0.619148	0.104432	0.002099	0.010099
0.58763	0.105407	0.001099	0.007296
0.556123	0.102321	0.000395	0.004704
0.524605	0.096802	0	0
0.493099	0.089148		

3.3 Impact of the Air Supply Method

One can find a puzzle related to cavitating flows over this hydrofoil in Fig. 13: while the C_D dependencies on σ for natural and ventilated cavitation are quite close, the dependencies of lift coefficients for two kinds of cavitation are not. Moreover, the method used to maintain ventilated cavitation at the constant σ affects the lift values.

The first method to vary σ during water tunnel tests carried out by Amromin et al. (2006) was based on a variation of the inflow pressure with the constant air supply. The drag minimum practically coincides with inherent to natural cavitation, whereas the lift maximum is substantially lower.

The second method was based on a variation of this supply with the constant inflow pressure (this method looks closer to the method employable in the full-scale conditions, but the inflow speed was also constant in the tests). No lift peak was measured for the second method. Why?

Also, as shown by Shao et al. (2018), an increase of air supply to the cavity can prevent its collapse, though the cavity would be highly pulsating. What are the threshold air supply rates?

Table 2 Lower side of hydrofoil OK2003

x/C	y/C	x/C	y/C
0	0	0.524605	-0.0634
0.000395	-0.0047	0.556123	-0.0605
0.001099	-0.0073	0.58763	-0.0574
0.002099	-0.0101	0.619148	-0.0542
0.003605	-0.0131	0.650667	-0.0506
0.005901	-0.0166	0.682173	-0.0469
0.009395	-0.0206	0.713691	-0.043
0.014605	-0.0254	0.745198	-0.039
0.022395	-0.031	0.776716	-0.0348
0.034198	-0.0376	0.808235	-0.0304
0.051901	-0.0451	0.839741	-0.0258
0.08342	-0.05458	0.871259	-0.0211
0.114926	-0.06121	0.902778	-0.0163
0.146444	-0.06611	0.934284	-0.0112
0.177951	-0.06958	0.965802	-0.0059
0.209469	-0.07205	0.977605	-0.0039
0.240988	-0.07351	0.985395	-0.0026
0.272494	-0.07435	0.990605	-0.0016
0.304012	-0.07458	0.994099	-0.001
0.335519	-0.07414	0.996395	-0.0006
0.367037	-0.07317	0.997901	-0.0004
0.398556	-0.07189	0.998901	-0.0002
0.430062	-0.07035	0.999605	0
0.46158	-0.06837	1	0
0.493099	-0.06604		

Another example of the impact of air supply method related to the “wavy” ventilated cavities was noted by Gorbachev and Amromin (2012): for the lower air demand, it is necessary to start the creation of such cavity from its tail. This unsteady phenomenon has no theoretical (computational) explanation. Also, there is no quantitative description of the process of cavity creation described by Arndt et al. (2009) and illustrated here in Fig. 13.

3.4 Wave Impact on Ships with Ventilating Cavities

The wave impact on ventilated cavities is also a substantial concern of naval architects. There are various effects of sea waves on the ships with such cavities.

One effect is the breakup of large “wavy” cavities under the ships operating at the small Froude numbers. Such breakup may occur due to either the direct impact of high magnitude waves or as a result of the ship pitch oscillations in waves.

Another effect is the mitigation of the wave-induced vertical acceleration by the “smooth” bottom ventilated cavities. This effect was observed at the bigger Froude numbers. At such Fr , the ventilated cavity can also reduce

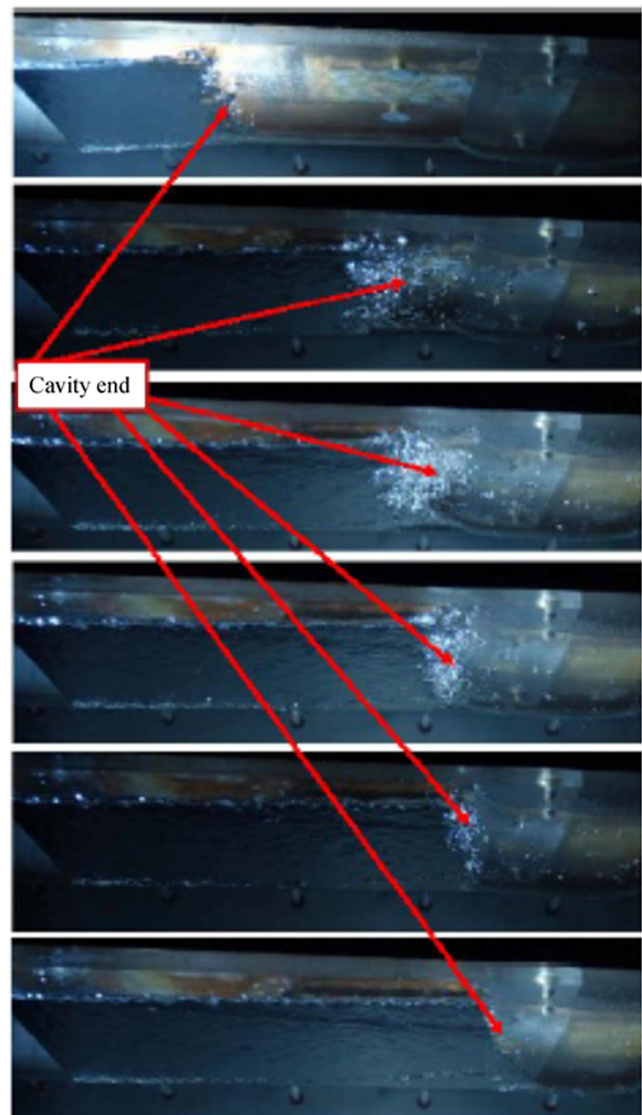


Fig. 14 Cavity creation under floor of the water tunnel at flow speed $U = 1.1$ m/s. Air supply rate $Q_c = 0.5$ liter per minute; dt is the cavity creation time, photos were made with the time step $dt/5$

the ship additional wave-induced resistance (in the moderate sea states allowing for the cavity maintenance). The computational attempt of Amromin (2018) to describe this effect in 2D approach (for the buttock of the Model 5494) was carried out using theory of ideal incompressible fluid for the water flow outside the cavity, but the compressible flow in the cavity was also considered there (consequently, the boundary conditions (2) and (3) were modified). As shown in Fig. 15, the mentioned mitigation was computationally proven for the ratios of the wavelength to the ship length $\lambda/L > 0.8$ (and this computed range of λ/L corresponds to the observations of Sverchkov (2005) for planning boats). However, this attempt delivered rather a qualitative analysis. So, it validates the selection of the flow model only.

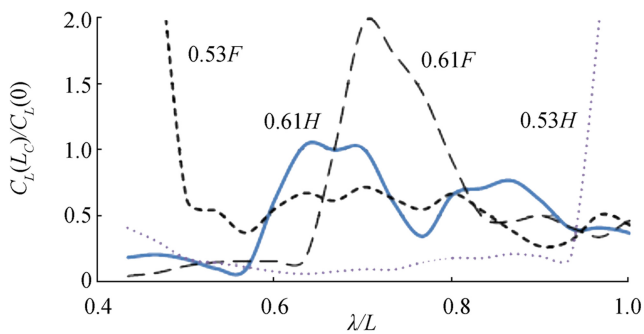


Fig. 15 Computed ratios of lift pulsation magnitudes for a ship with bottom cavities and w/o them; 0.53F means the dependency for $Fr = 0.53$ in following sea, 0.61H—for $Fr = 0.61$ in head seas, etc.

As seen in Fig. 16, there is the quantitative difference between 2D and 3D cavitation even for hydrofoils with the same sections. Also, the results presented in Fig. 15 were not obtained from the complete solution for the hull motion in waves: the experimental data on the time-average pitch and heavy were used in these computations.

The quantitative 3D analysis with the complete computation of the flow around the ship with cavity and the ship dynamics is the unsolved problem yet. Possibly, the existing hydrodynamic software packages can be extended to include new solvers.

3.5 Ventilation and Impact of Shock Waves in Cavities

Shock wave as the mechanism of cavitation induced erosion has been discussed for decades. One can find the corresponding notes in the book of Knapp et al. (1970), but the wave appearance was addressed to a collapsing bubble. Also, these notes were not supported by computations capable of proving the concept associated with the collapse of a bubble in the pure water. Recently, Jian et al. (2015) and Usta et al. (2017) gave satisfactory predictions of the erosion areas, but not the body mass losses due to erosion. So, the physical mechanism of erosion was not clarified yet.

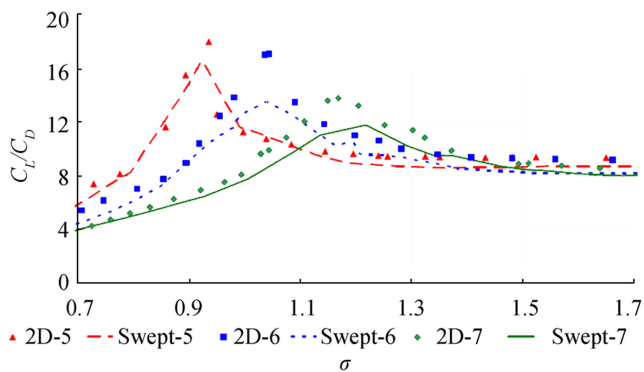


Fig. 16 Comparison of lift to drag ratio for 2D and swept hydrofoils with sections OK2003 at various angles of attack; 2D-5 are experimental data for 2D hydrofoil at $\alpha = 5^\circ$, etc.

On the other hand, Amromin (1990) supposed that the shock waves of sufficient intensity may appear in the homogeneous gas-water mixture within the cavity tail and be amplified due to the interaction of these waves with the metal used for body fabrication. Later Reisman et al. (Reisman et al. 1998) found shock waves in their experiments with cloud cavitation and Ganesh et al. (2016) described the shock waves observed within sheet cavities.

As shown below, ventilation can reduce the impact of shock waves generated in the cavity and propagating to the bodies. An analysis of their generation and interaction with the solid body is given here for a cavitating hydrofoil in the one-dimensional approach. The sketch of wave propagation in the direction perpendicular to hydrofoil surfaces is presented in Fig. 17 (z is the coordinate counted along the normal to its surface). There are three media participating in this interaction: water on one hydrofoil side, water-gas mixture on another, and metal between them. As shown in this sketch, the interaction of shock waves with various media can lead to diffraction and propagation of different kinds of waves. The velocities and pressure are continuous on the boundary between media (on contact surfaces), whereas these flow characteristics experience a jump on the shock wave fronts.

First of all, it is necessary to point out the conditions of the shock wave generation in the cavity. As seen in the photos published by Ganesh et al. (2016), the reentrant jet acts as a piston and can generate a shock wave when its velocity U_S exceeds the local sound speed c . In a water-gas mixture, this speed is defined as

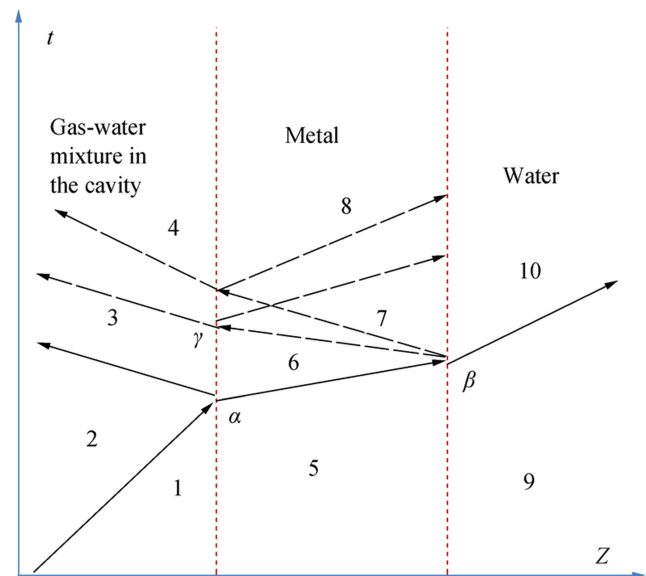


Fig. 17 Sketch of shock wave interaction with a cavitating hydrofoil; dashed lines are its surfaces; solid arrows are shock wave trajectories in the $\{z, t\}$ plane, dashed arrows limits rarefaction wave images in this plane

$$c = \left(\frac{m}{\rho_g} + \frac{1-m}{\rho_w} \right) / \sqrt{\left(\frac{1}{\rho_g c_g} \right)^2 m + (1-m) \left(\frac{1}{\rho_w c_w} \right)^2} \quad (4)$$

Here, m is the gas mass concentration, the subscripts “g” mark the gas characteristics and “w” the water characteristics. The formula $p_2 = II\rho_w U^2$ can link pressure behind the shock wave with the inflow speed U . According to the data provided by Tran et al. (2015), $0.2 < II < 0.6$; here, $II = 0.5$ is used. Some results of the calculation of sound speed in vapor-water and air-water mixtures with the use of Eq. (4) are shown in Fig. 18. For the same void fraction v , the sound speed is lower in vapor. So, ventilation can delay the generation of shock waves.

As shown, the evolution of the supersonic flow within the cavity depends also on the material used in hydrofoil fabrication. The difference in the type of wave interaction between two media is caused by the difference in their densities and sound speeds. Densities ρ of the pure media are described by Tait equation:

$$\left(\frac{\rho}{\rho_0} \right)^\kappa = \frac{P+B}{P_0+B} \quad (5)$$

The coefficients of Eq. (5) are individual. The coefficients for metals were calculated in Table 3 using the experimental data of Al'tshuler and Bakanova (1969). The corresponding sound speeds are also in Table 3.

As described by Courant and Friederichs (1948), the jump of the media velocity on the shock wave front can be linked to the jumps of pressure and density. In particular, the velocity jump on the shock waves within the mixture is

$$F_{2,1} = (p_2 - p_1) \sqrt{\frac{m}{\rho_{a1} \Omega(p_2, p_1)} + \frac{(1-m)}{\rho_w \kappa_w (B_w + p_2)}}$$

Here and below, subscripts at pressure and densities indicate zones in Fig. 17, $\Omega(p_2, p_1) = (\kappa_g + 1)p_2 + (\kappa_g - 1)p_1$. For the same p_2 , the velocities behind the wave are different in nature and ventilated cavities because of the difference of

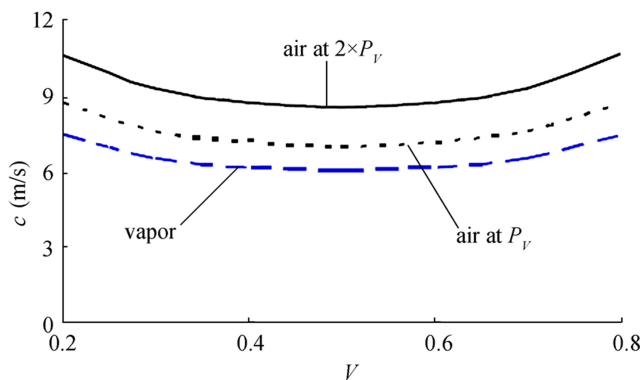


Fig. 18 Dependencies of the mixture sound speed on its void fraction

Table 3 Coefficients of Eq. (5) and sound speeds of various materials at atmosphere pressure

Material	κ	B (Pa)	$C = (\kappa B/\rho)^{0.5}$ (m/s)
Aluminum	5.3	1.09×10^{10}	4618
Cooper	5.65	2.25×10^{10}	3756
Water	7.0	3.07×10^8	1492
Vapor	1.29	0	406
Air	1.42	0	340

sound speed and density for water vapor and air. So, as seen in Fig. 19, the Mach numbers $M = F_{2,1}/c$ are lower for the air-water mixture with the same U even for a higher p_1 usually inherent to ventilated cavities. Because there will be no shock wave at $M < 1$, ventilation would delay erosion (will increase its threshold speed).

At the point α of the $\{z, t\}$ plane (but in a fixed hydrofoil point, see Fig. 17), the shock wave will propagate in the metal and a diffracted shock will go to the fluid. The interaction in this point for the vapor cavity is described by the equation

$$A_M(p_3 - p_1) = F_{2,1} - (p_3 - p_2)A_w \quad (6)$$

Here, p_3 is the unknown quantity, $A_M = 1/\sqrt{\rho_M B_M \kappa_M}$ and $A_w = 1/\sqrt{\rho_w B_w \kappa_w}$, and subscript “M” relates to the metal. The left-hand side of Eq. (6) is the velocity on the right side of the contact surface, and its right-hand side, on its left side. For the air cavity, Eq. (6) has the form

$$A_M(p_3 - p_1) = F_{2,1} - (p_3 - p_2) \sqrt{(1-m)A_w + \frac{m\Omega(p_1, p_2)}{\rho_{a1}\Omega(p_2, p_1)\Omega(p_3, p_2)}}$$

In both situations, this condition can be used to determine p_3 . Calculations show that for any metal $p_3 \gg p_2$.

Further, the shock wave will go to the water on another side of the hydrofoil, but the diffracted wave will be the rarefaction wave with the change of the media velocity $f(p_2, p_4) = \int_{p_2}^{p_4} \frac{dp}{\rho c}$.

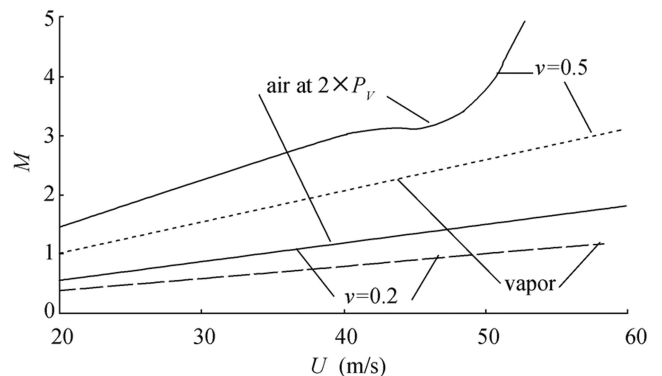


Fig. 19 Dependencies of Mach number on the inflow speed for vapor and ventilated cavities

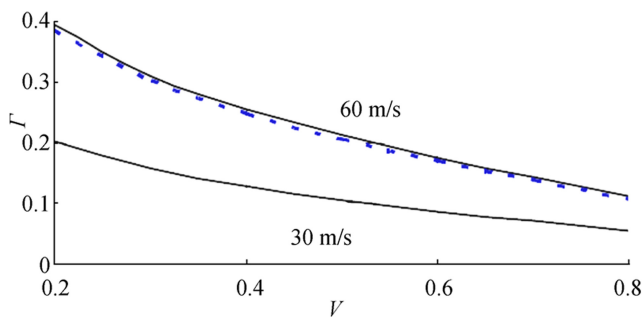


Fig. 20 Ratio of shock wave mitigation by ventilation for the cavity pressure $p_1 = 2P_*$. Solid lines relate to aluminum foil, dotted line—to cooper foil

So, the pressure P_{10} related to the rarefaction wave returning to the surface under the cavity can be found from the equation

$$\frac{c_M(p_3 - P_{10})}{(2\kappa_M - 1)B_M \kappa_M} + A_w(p_{10} - p_9) = F_{3,1}$$

and $p_{10} = p_7 < p_3$. The ratios Γ of p_{10} for a ventilated cavity to its value in the vapor cavity is shown in Fig. 20. Ventilation substantially mitigates this pressure.

Let us, however, recall that dependencies in Figs. 19 and 20 were obtained with several substantial simplifications of the phenomenon. These dependencies do not take into account the three-dimensional character of wave propagation, the approximate value used for Π , non-uniformity, and stochastic nature of void fraction distribution within the cavities. So, an accurate CFD analysis of erosion mitigation by ventilation is necessary.

4 Conclusions

This paper recalls the successful applications of ventilated cavitation to naval engineering, briefly estimates state-of-the-art in the related branch of computational fluid dynamics and emphasizes several computational problems appeared from the experiments with the ship models, full-scale ships and hydrofoils with the ventilated cavities. This emphasis is also supplemented by several experimental and computational results that were not published yet.

It is pointed out that the major successes in the application of ventilated cavitation as the drag reduction technology was substantially based on the solutions of design problems solved in the framework of ideal fluid theory. However, it is also accentuated that the interaction of the cavities with the surrounding viscous flow and their effect on the total drag cannot be predicted by this theory.

As also noted, design validation by the model test is usually carried out keeping similarity by Froude number, whereas air demand by cavities is certainly affected by the surrounding turbulent boundary layers. Prediction of this demand and its

dependency on air supply methods remain to be unsolved problems for both ship hulls and ventilated hydrofoils. The wave impact on ships on ventilated cavities and the cavity influence of wave-induced loads on the ships should be determined from solutions of CFD problems, as well. The above-mentioned problems would be serious topics for future CFD studies.

Besides, as explained in the paper, ventilation can be used as an erosion control technique. The provided analysis of shock wave propagation within the cavities found the ventilation effect on this propagation, but it also found the impact of hydrofoil material on these waves.

The paper also includes detailed information on the innovative hydrofoil OK2003 and experimental data on its cavitation. Its natural and ventilated cavitation looks like the perfect novel benchmark problem for CFD solvers.

References

- Abolfazl S, Leer-Anderson M, Bensow RE, Norrby J (2012) Hydrodynamics of a displacement air cavity ship. *29th Symp. Naval Hydrodynamics*, Gothenburg, Sweden
- Al'tshuler LV, Bakanova AA (1969) Electronic structure and compressibility of metals at high pressures. *Sov Phys Usp* v11:678–689
- Amromin EL (1990) On the nature of threshold velocity for cavitation erosion. *Scientific and Methodological Seminar on Ship Hydrodynamics*, Varna, Bulgaria
- Amromin EL (2007) Analysis of body supercavitation in shallow water. *Ocean Eng* 34:1602–1606
- Amromin EL (2018) Ship bottom cavity as shock absorber in waves. *J Mar Sci Appl* 17:173–177. <https://doi.org/10.1007/s11804-018-0019-3>
- Amromin EL, Arndt REA (2019) Analysis of influence of cavity content on flow pulsations. *Int J Multiphase Flow* 110:108–117
- Amromin EL, Kopriva J, Arndt REA, Vosnik M (2006) Hydrofoil drag reduction by partial cavitation. *ASME J Fluids Engineering* 128: 931–936
- Amromin EL, Metcalf B, Karafiath G (2011) Synergy of resistance reduction effects for a ship with bottom air cavity. *ASME J Fluids Engineering* 133:021302(1)–021302(7)
- Arndt REA, Hambleton J, Kawakami E, Amromin EL (2009) Creation and maintenance of cavities under horizontal surfaces. *ASME J Fluids Engineering* 131:111301(1)–111301(10)
- Basin A, Butuzov A, Ivanov A, Olenin Y, Petrov V, Potapov O, Ratner E, Starobinsky V, Eller A (1969) Operational tests of a cargo ship 'XV VLKSM congress' with air injection under a bottom. *River Transport:52–53 in Russian*
- Butuzov AA (1966) Extreme parameters of vented cavity on the top surface of horizontal wall. *Fluids Dynamics:167–170*
- Butuzov AA, Gorbachev YN, Ivanov AN, Kaluzhny VG, Pavlenko AN (1990) Ship drag reduction by artificial gas cavities. *Sudostroenie* 11:3–6 in Russian
- Choi J-K, Chahine GL (2010) Numerical study on the behavior of air layers used for drag reduction. *28th Symp Naval Hydrodynamics*, Pasadena, California, USA
- Compendium on naval hydrodynamics* (2015) Paris, France: ENSTA
- Courant R, Friederichs KO (1948) *Supersonic flow and shock waves*. Interscience Publ, NY

- Courouble M (1971) Recherche sur une technique de reduction de la resistance a la marche des navires lents. ATMA-1971 Conf, Paris (in French)
- Coutier-Delgosha O, Devillers J-F, Pichon T (2006) Internal structure and dynamics of sheet cavitation. *Phys Fluids* 18:017103. <https://doi.org/10.1063/1.2149882>
- Foeth EJ (2008) Decreasing of frictional resistance by air lubrication. *20th Int Symposium on Yacht Design and Yacht Construction*, Amsterdam, NL
- Ganesh H, Makiharju SA, Ceccio SL (2016) Bubbly shock propagation as a mechanism for sheet-to-cloud transition of partial cavities. *J Fluid Mech* 802:37–78
- Gorbachev YN, Amromin EL (2012) Ship drag reduction by ventilation from Laval to near future: challenges and successes. *Conference of Association Technique Maritime et Aeronautique*, Paris
- Gorbachev YN, Sverchkov AV, Galushina MV (2015) Propulsion of displacement ships with the single bottom cavities. *Sudostroenie* 1: 17–23 in Russian
- Gurevich MI (1970) Theory of jets in ideal fluids. AC Press, NY
- Ji B, Luo X, Peng X, Zhang Y, Y-l W, Xu H (2010) Numerical investigation of the ventilated cavitating flow around an underwater vehicle based on a three-component cavitation model. *J Hydrodyn* 22: 753–759
- Jian W, Petkovšek M, Houlin L, Širok B, Dular M (2015) Combined numerical and experimental investigation of the cavitation erosion process. *ASME J Fluids Eng* 137:051302
- Kim S-E (2015) Progress in numerical simulation of turbulent cavitating flow in an axial waterjet pump. *J Phys Conf Ser* 656:012064
- Kinzel MP, Lindau JW, Peltier J, Zajaczkowski F, Arndt REA, Wosnik M, Mallison T (2007) Computational investigation of air entrainment, hysteresis and loading for large-scale, buoyant cavities. *NMSH2007 Conf*, Ann Arbor, 3, 306
- Knapp RT, Daily JW, Hammitt FG (1970) Cavitation, McGraw-Hill
- Kopriva J, Amromin EL, Arndt REA, Kovinskaya SI (2007) High performance partially cavitating hydrofoils. *J Ship Res* 51:313–325
- Kubota A, Kato H, Yamagushi H (1992) A new modeling of cavitating flows: a numerical study of unsteady cavitation of a hydrofoil section. *J Fluid Mech* 240:59–96
- Kuklinski R, Henoch C, Castano J (2001) Experimental studies of ventilated cavities on dynamic test model. *Cav-2001 Symposium*, Pasadena
- Latorre R (1997) Ship hull drag reduction using bottom air injection. *Ocean Eng* 24:161–175
- Liu T, Huang B, Wang G, Zang M (2018) Experimental investigation of ventilated partial cavitating flows with special emphasis on flow pattern regime and unsteady shedding behavior around an axisymmetric body at different angles of attack. *Ocean Eng* 147:289–303
- Long Y, Long X, Ji B, Huai W, Qian Z (2017) Verification and validation of URANS simulations of the turbulent cavitating flow around the hydrofoil. *J Hydrodyn* 29:610–620
- Mäkiharju S, Elbing BR, Wiggins A, Dowling DR, Perlin M, Ceccio SL (2010) Perturbed partial cavity drag reduction at high Reynolds numbers. *28th Sym. Naval Hydrodynamics*, Pasadena, USA
- Matveev KI (2007) Three-dimensional wave patterns in long air cavities on a horizontal plane. *Ocean Eng* 34:1882–1891
- Reichardt H (1945) Die Gesetzmäßigkeiten der Kavitationsblasen an umströmten Rotationskörpern, Göttingen UM, 6628 (in German)
- Riesman GF, Wang Y-C, Brennen CE (1998) Observation of shock waves in cloud cavitation. *J Fluid Mech* 355:255–283
- Shao S, Wu Y, Haynes J, Arndt REA, Hong J (2018) Investigation into the behaviors of ventilated supercavities in unsteady flow. *Phys Fluids* 30:052102. <https://doi.org/10.1063/1.5027629>
- Sverchkov AV (2005) Prospects of artificial cavities in resistance reduction for planning catamarans with asymmetric demihulls. *International Conference on Fast Sea Transport FAST'2005*, St. Petersburg, Russia
- Sverchkov AV (2010) Application of air cavities on high-speed ships in Russia. *Intern Conf ship drag reduction*, Istanbul
- Thill C (2010) A long road mapping drag reduction. *Intern Conf on Ship Drag Reduction*, Istanbul
- Tran DT, Nennemann B, Vu TC, Guibault F (2015) Investigation of cavitation models for steady and unsteady cavitating flow simulation. *Intern J Fluid Mach Syst* 8:240–253
- Usta O, Aktas B, Maasch M, Turan O, Atlar M, Korkut E (2017) A study on the numerical prediction of cavitation erosion for propellers. *5th Int Symp Marine Propulsion*, Espoo, Finland
- Wang Z, Huang B, Wang G, Zhang M, Wang F (2015) Experimental and numerical investigation of ventilated cavitating flow with special emphasis on gas leakage behavior and re-entrant jet dynamics. *Ocean Eng* 108:191–201
- Wosnik M, Schauer T, Arndt REA (2003) Experimental study on a ventilated supercavitating vehicle. *5th Int Sym Cavitation*, Osaka, Japan
- Xiang M, Cheung SCP, Tu JY, Zhang WH (2011) Numerical research on drag reduction by ventilated partial cavity based on two-fluid model. *Ocean Eng* 38:2023–2032
- Young JL, Harwood CM, Montero FM, Ward JC, Ceccio SL (2017) Ventilation of lifting bodies: review of the physics and discussion of scaling effects. *Appl Mech Rev* 69:010801. <https://doi.org/10.1115/1.4035360>
- Zverkovski O, Terwisga T, van Gusing M, Westerwell J, Delfos R (2014) Experimental study on drag reduction by air cavities on a ship model. *30th Sym Naval Hydrodynamics*, Tasmania